# High-temperature kinetic isotope fractionation of calcium in epidosites from modern and ancient seafloor hydrothermal systems

Shaun T. Brown[1,2], Alexandra V. Turchyn[3], Mike J. Bickle[3], Amy C. Davis[3,#], Jeffrey C. Alt[4], Jean H. Bédard[5], Thomas Skulski[6] and Donald J. DePaolo[1,2*]

1. Dept of Earth and Planetary Science, University of California, Berkeley, Berkeley, CA 94720

2.Energy Geosciences Division, E.O. Lawrence Berkeley Laboratory, Berkeley, CA 947203.

3. Department of Earth Sciences, Downing Street, University of Cambridge, Cambridge CB2 3EQ United Kingdom

4. Dept of Earth and Environmental Sciences, University of Michigan, Ann Arbor, MI 48109

5. Geological Survey of Canada, 490 de la Couronne, Québec, Qc, Canada, G1K 9A9

6. Geological Survey of Canada, Natural Resources Canada, 601 Booth Street, Ottawa, Ontario, Canada, K1A 0E8

*corresponding author: depaolo@eps.berkeley.edu

Keywords: epidote, calcium isotopes, ophiolite, hydrothermal mineralization, kinetic isotope fractionation, reactive transport

**Abstract**

Calcium isotope ratios in epidote from epidosites in ophiolites of varying Phanerozoic ages have $^{44}Ca/^{40}Ca$ ratios that are lower by 0.1 to 0.6‰ relative to typical mid-ocean ridge hydrothermal fluids. Epidosites are inferred to form in high- temperature parts of seafloor hydrothermal systems at temperatures above 300°C and where fluid fluxes are high, so the Ca isotopic composition of the epidote is likely to reflect fractionation during growth of crystals

from aqueous solution. Available Ca isotope data from MOR hydrothermal vent fluids and mantle peridotites constrain the $\delta^{44}Ca$ of likely modern hydrothermal fluids to a narrow range at $\delta^{44}Ca = -0.05 \pm 0.1$. A reactive-transport model is used to evaluate whether the $\delta^{44}Ca$ of hydrothermal fluids might have been higher during the Cretaceous and Late Cambrian, the ages of the Troodos, Oman, and Betts Cove ophiolites from which we have data. For these calculations we use the epidosite $^{87}Sr/^{86}Sr$ as a guide to the extent of Ca isotopic exchange that affected the ancient hydrothermal fluids, which were derived from seawater with higher Ca and Sr, and lower sulfate concentration, than modern seawater. The calculations suggest that the ancient hydrothermal fluid $\delta^{44}Ca$ values were not much different from modern values, with the possible exception of the Late Cambrian example. We infer that the epidote-fluid Ca isotope fractionation averaging $\Delta^{44}Ca = -0.2$ to $-0.6$, is most likely due to kinetic isotope fractionation during mineral precipitation. There is evidence from the literature that hydrothermal epidote may commonly form from oversaturated solutions, which makes the kinetic isotope interpretation plausible. The equilibrium epidote-fluid Ca isotope fractionation is estimated to be $\Delta^{44}Ca_{eq} \approx 0$ based on recently reported DFT calculations. Our results suggest that kinetic calcium isotope fractionation can affect hydrothermal silicate minerals, and may be only slightly smaller in magnitude than the effects observed in Ca-bearing minerals at low temperature. Kinetic isotope effects during mineral growth could provide new insights into the formation mechanisms of hydrothermal silicate minerals.

## 1. Introduction

### *1.1 Ophiolites as representatives of ancient mid-ocean ridge hydrothermal systems*

A significant mechanism for heat and mass transfer from the solid Earth to the oceans and atmosphere is the hydrothermal alteration of oceanic crust at mid-ocean ridges. Seawater circulation at mid-ocean ridges is responsible for 20% of the Earth's heat loss (C. A. Stein and S. Stein, 1994) and affects seawater chemistry, adding significant amounts of base metals, removing Mg and $SO_4$ and adding Ca, and probably controlling the oxygen isotopic composition of the oceans on geologic timescales (Elderfield and Schultz, 1996; Gregory, 2003). In addition, altered oceanic crust imparts distinct chemical (e.g. K and Ce/Pb) and isotopic (e.g. $^{87}Sr/^{86}Sr$ and $\delta^{18}O$) signatures to island arc lavas (Kay, 1980; Kay et al., 1978; Miller et al., 1994; Staudigel and Hart, 1983) and with deep subduction, modifies the chemical composition of the deep mantle (Hofmann and White, 1982; White, 2015).

Interest in hydrothermal alteration of the oceanic crust initially was motivated by study of dredged rocks (Hart, 1969; Humphris and Thompson, 1978), the discovery of ocean ridge hydrothermal vents (Corliss et al., 1979) and the recognition that ophiolites are obducted portions of oceanic crust that once experienced hydrothermal alteration (Gass, 1968; Moores and Vine, 1971). Subsequent field and laboratory research has probed high temperature hydrothermal alteration of the oceanic crust and its effect on the chemical composition of seawater (Alt and Teagle, 2000; Bach and Fruh-Green, 2010; Berndt et al., 1989; Bickle and Teagle, 1992; Damm, 2000; Seyfried and Mottl, 1982; Seyfried et al., 2011). This research has included studies of active vent fluids (von Damm, 2000), scientific drilling in oceanic crust (Alt and Teagle, 2003; Pritchard, 1979; Staudigel, 2003) and studies of obducted sections of oceanic crust (Bickle and Teagle, 1992; Coogan, 2009; Gregory, 2003). Ophiolites offer the opportunity

to sample a nearly continuous section of crust from the extrusive basalts through to the inferred magma source region and are critical for our understanding of the geometry and chemistry of ocean ridge hydrothermal systems as drilling into modern oceanic crust has only just penetrated into the top of the gabbros.

Ophiolites are important analogues of oceanic crust as evidenced by similarities with the one-dimensional seismic structure of oceanic crust (Christensen, 1978); evidence of sheeted dykes in deep-sea drilling and submarine escarpments (Karson, 2016); similarity between seafloor hydrothermal vents and alteration and ophiolite-hosted volcanogenic massive sulfide deposits and their root zones (Richardson et al., 1987). However, the composition of many volcanic rocks within ophiolites suggest that most ophiolites did not form in a mid-ocean ridge setting, and may have formed in various supra-subduction zone settings (Dilek and Furnes, 2014). The relevance of ophiolite fossil hydrothermal systems to mid-ocean ridge processes thus is tempered by potential differences in their tectonic settings and magmatic character. In any case, the rocks were hot, fractured, composed largely of basalt and diabase where the alteration is strongest, and the hydrothermal fluid was almost certainly derived from seawater.

*1.2 Ca and Ca isotopes in mid-ocean ridge hydrothermal systems*

Calcium is one of three major constituents of seawater other than Na and Cl, the other two being Mg and $SO_4$. The typical evolution of seawater-derived hydrothermal fluid in seafloor systems is that first, Mg and $SO_4$ are removed from the fluids, as evidenced by the absence of Mg and $SO_4$ in high temperature vent fluids. The removal of $SO_4$ is largely by precipitation of anhydrite ($CaSO_4$), and the removal of Mg is due to the insolubility of Mg-rich secondary minerals like chlorite, tremolite, and montmorillonite, which precipitate rapidly once

93 sufficient Al, Ca, and Si are provided by dissolution of the primary igneous silicate minerals.
94 Calcium on the other hand, increases in concentration to compensate for the loss of Mg and
95 $SO_4$, effectively preserving charge balance of the evolving hydrothermal fluid (Antonelli et al.,
96 2017). The Ca concentration of vent fluids is up to 5 times higher than the concentration in
97 modern seawater (vonDamm 2000), therefore in the hydrothermal system there is a large
98 contribution of rock-derived Ca to the fluid. Any 'original' seawater Ca in modern systems is
99 largely removed by anhydrite precipitation at temperatures above 150°C, prior to and partly
100 concurrent with the fluid reaching the highest temperature parts of the system. Consequently, it
101 is generally inferred that almost all of the Ca in modern high temperature seafloor hydrothermal
102 fluids is derived from the rocks (Scheuermann et al., 2018). This inference is consistent with
103 the generally low $^{87}Sr/^{86}Sr$ values in modern high temperature vent fluids, but may not apply to
104 seafloor hydrothermal systems of Cretaceous and early Paleozoic age when the relative
105 seawater concentrations of Ca, Mg and $SO_4$ were different (Lowenstein et al., 2014; Antonelli et
106 al., 2017).
107 The seawater that interacts with oceanic crust in mid-ocean ridge or supra subduction
108 zone settings evolves in composition as a function of chemical interaction (partial dissolution of
109 primary igneous minerals like olivine, pyroxenes and plagioclase, and precipitation of
110 secondary minerals such as anhydrite, montmorillonite, amphibole, albite, and chlorite). Many
111 studies have concluded that the chemical compositions of high-temperature hydrothermal vent
112 fluids indicate that the fluids get close to chemical equilibrium with the igneous minerals in the
113 parts of the systems where temperatures are at or above 400°C (Pester et al., 2012; Seyfried and
114 Ding, 2013). Studies of $^{87}Sr/^{86}Sr$ from the sheeted dykes of ophiolites and modern ocean crust
115 indicate incomplete Sr isotopic exchange between MORB and hydrothermal fluids (Bickle and

116 Teagle, 1992; Coogan, 2009; Harris et al., 2015; DePaolo, 2006; Turchyn et al., 2013). The
117 $^{87}Sr/^{86}Sr$ of modern ridge vent fluids are also typically different from (higher than) the host
118 rocks, consistent with the observations from ophiolites. The observed differences in $^{87}Sr/^{86}Sr$
119 are not inconsistent with nearly-equilibrated fluid chemical composition; instead they indicate
120 that $^{87}Sr/^{86}Sr$ preserves information about the extent of fluid-rock interaction that is not
121 available from the fluid chemical compositions.

122 *1.3 Epidosites in mid-ocean ridge hydrothermal systems*

123 Epidosites are epidote-quartz-sphene rocks representing extreme alteration of basalt at
124 temperatures of 300 to 400 °C (Richardson et al., 1987; Schiffman et al., 1987). Epidosites form
125 from fluids flowing in fractures or highly altered high porosity zones where the time integrated
126 fluid flux is high (Bickle and Teagle, 1992; Cann et al., 2014). Hence, the epidote in epidosites
127 is likely to have formed by precipitation directly from high-temperature hydrothermal fluids.
128 We studied hydrothermal epidote from epidosites from ophiolites, and epidote-quartz veins
129 recovered during ODP drilling, with the intention of using epidote to measure the Ca isotopic
130 composition of ancient hydrothermal fluids, assuming that there was no Ca isotopic
131 fractionation between epidote and fluid at 300° - 400°C. The hydrothermal epidotes we
132 measured, however, have lower $\delta^{44}Ca$ than are likely for hydrothermal fluids. Our
133 interpretation of this observation, discussed in detail below, is that there is calcium isotopic
134 fractionation during epidote formation, and that it represents a kinetic isotope effect (KIE)
135 associated with non-equilibrium growth of epidote from hydrothermal solutions (cf. Watkins et
136 al., 2017). This conclusion, if correct, has important implications for the way we understand
137 mineral formation from high temperature fluids..

138

## 2. Sample Selection and Background

Epidosite veins, consisting primarily of quartz and epidote, were collected from sheeted dykes from Troodos (91 Ma), Semail (95 Ma), Betts Cove (489 Ma), and epidote-quartz separates from veins in ODP Hole 504B (5.9 Ma). The sample localities were specifically targeted at veins with the highest fluid-rock ratios, given the size/width of the vein, and cross cutting relationships were used to target the oldest veins. The Betts Cove and Troodos samples were previously described by Turchyn et al (2013). A detailed description of the Oman epidosites is provided in the supplementary material. The 504B epidote separate is from 674 meters sub-basement (Alt et al., 1986). The $\delta^{18}O$ of epidote and quartz were reported by Alt et al (1986) and are similar to other epidote recovered in the 504B drill core, however the quartz separate has elevated $\delta^{18}O$, consistent with low temperature overgrowth (Alt, 1995b; Alt and Teagle, 2000). We estimated a fluid temperature of 325°C based on adjacent samples from the 504B core.

The analyzed epidotes are calcium-iron-aluminum silicates with negligible magnesium, sodium and potassium. Within the epidote group minerals, a solid solution exists between ferric iron and aluminum in one of the three M sites, and thus the compositions range between $Ca_2Al_3(SiO_4)_3OH$ and $Ca_2FeAl_2(SiO_4)_3OH_7$ (Armbruster et al., 2006). Epidote compositions were determined by electron microprobe at UC Berkeley (Turchyn et al., 2013) and are expressed as the mole fraction Fe relative to the total Fe and Al in the M crystallographic sites, subsequently referred to as the mole fraction pistacite (Xps). Xps varies by up to 20% among analyses for an individual sample, and the mean values for all samples are between 0.20 and 0.28.

Oxygen isotope ratios, reported as $\delta^{18}O$ (relative to the VSMOW standard), for quartz

and epidote and $^{87}Sr/^{86}Sr$ of some of the epidotes were previously reported in Turchyn et al. (2013). Fluid temperatures were calculated using the $\Delta^{18}O_{quartz-epidote}$ thermometer of Matthews and Schliestedt (1984). Calculated fluid temperatures range from 185 to 500°C with most temperatures between 300-400°C (Table 1). We focused our calcium isotope analysis on samples with quartz-epidote oxygen isotope thermometry temperatures >225°C, within the stability range for hydrothermal epidote (Bird and Spieler, 2004), to avoid possible effects of a low temperature overprint or disequilibrium.

## 3. Methods

Separated epidotes were dissolved on a 130°C hotplate with 0.5-1.0 ml of hydrofluoric and nitric acids in a 10:1 mixture. Dissolved samples were dried to completeness and dissolved in 6 M $HCl^-$. An aliquot for each sample containing 20 micrograms of calcium was spiked with a $^{42}Ca$-$^{48}Ca$ enriched tracer. The remaining dissolved epidote solutions were reserved for strontium isotope and Rb-Sr concentration measurements.

Aliquots for stable calcium isotopes were purified on Dowex AG50WX-8 cation exchange resin using nitric acid as the eluent. Purified calcium was loaded on double rhenium filaments in nitric and phosphoric acid. Samples were analyzed in the UC Berkeley ThermoFisher Triton TIMS. Calcium isotopes are measured as the ratio of $^{44}Ca$ to $^{40}Ca$ and reported versus a standard (either bulk silicate Earth, seawater or the carbonate standard 915A) in 'delta' notation.

$$\delta^{44}Ca = 1000\left[\frac{^{44}Ca/^{40}Ca_{measured}}{^{44}Ca/^{40}Ca_{std}} - 1\right] \quad (1)$$

Each reported value (Table 1) is based on three repeat analyses and the uncertainty quoted

184 reflects the reproducibility rather than the internal precision of a single analysis. The quoted
185 precision of ±0.04 to ±0.18, averaging ±0.10 is similar to or slightly larger than the average
186 (±0.08) we have obtained on hundreds of rock and mineral analyses over the past several years
187 (Antonelli et al., 2018, 2019a,b). In this paper, we report the $\delta^{44}Ca$ values relative to "bulk
188 silicate earth" or BSE as a reference. Combining our recent data on laboratory standards
189 (Antonelli et al, 2019), with the data on ophiolites reported in Kang et al. (2017) and Chen et al
190 (2019), we can confirm that our reference value is equal to the best current estimate for BSE.
191 As reported in Antonelli et al (2019), we measure the $\delta^{44}Ca$ of SRM915a to be -0.96 ±0.05
192 relative to our BSE reference value of $^{44}Ca/^{40}Ca = 0.0212094$. Kang et al. (2017) and Chen et al
193 (2019) have determined a best estimate value for the $\delta^{44}Ca$ of BSE based on lherzolites and
194 clinopyroxene-rich ophiolite rocks to be +0.94 ± 0.05. Hence our reference value for $^{44}Ca/^{40}Ca$
195 is almost exactly equal to the best current estimate for BSE. Relative to other standards, our
196 BSE standard value is 0.95 ±0.05 units lower than seawater and 0.96 ±0.05 units higher than
197 SRM915a (on our scale, seawater has $\delta^{44}Ca = +0.95$ and SRM986 has $\delta^{44}Ca = -0.96$; also see
198 Figure 2).

199 Although others have argued for using seawater or the SRM915a standard to report $\delta^{44}Ca$
200 values, we use the BSE value as the reference, because it has petrological and planetary
201 significance and is invariant with geologic time (Nielsen et al., 2011). This general approach
202 has been commonly used in stable isotope geochemistry. For example, silicate $\delta^{18}O$ values are
203 normally reported relative to SMOW ("standard mean ocean water"), but the laboratory
204 standard used is not ocean water (which has variability in any case), but rather an in-house
205 silicate standard whose value relative to SMOW has been agreed upon by convention or
206 demonstrated in the lab. We use the SRM915a standard as an internal laboratory standard, but

we have established that the BSE value is 0.96±0.05‰ higher than SRM915. Any uncertainties caused by this renormalization are smaller than the ~ ±0.1‰ uncertainties of the analyses.

Epidotes from Betts Cove, Troodos and 504B were measured for $^{87}Sr/^{86}Sr$ following the same protocol as Turchyn et al (2013). Dissolved samples were loaded on cation exchange columns containing Dowex AG50W-X8 resin and strontium was purified using conventional $HCl^-$ cation exchange techniques. Strontium chemistry blanks were better than 20 pg, which obviates the need for blank corrections. Purified strontium was loaded on single rhenium filaments in 1% $H_3PO_4$ and a $TaCl_5$ activator. Mass discrimination was corrected in- run to $^{86}Sr/^{88}Sr$ of 0.1194. During the course of this study NBS987 yielded 0.71024 ± 0.00001 (2σ). Most epidote separates have $^{87}Rb/^{86}Sr < 0.0013$, but for samples where the $^{87}Rb/^{86}Sr$ is >0.0013 age corrected $^{87}Sr/^{86}Sr$ are reported (Table 1).

The Oman epidosite samples were analyzed at Cambridge following the methods of Bickle et al (2003) using cation exchange chromatography to purify Sr. Analyses at Cambridge utilized a VG54E TIMS using a dynamic triple collector algorithm and normalized to $^{86}Sr/^{88}Sr = 0.1194$ with an exponential fractionation correction. Repeat analyses of standard NBS-987 gave a mean $^{87}Sr/^{88}Sr = 0.710247 \pm 11$ (2σ, n=51) during the period the samples were analysed. Chemical processing blanks were always < 1 ng (mostly <100 pg) which is negligible given that > 15 μg of Sr was separated from 0.15 g of rock powders.

## 4. Results

The measured $\delta^{44}Ca$ of hydrothermal epidotes span -0.11 in to -0.56 relative to BSE (**Fig 1, 3**). All fourteen of the samples have $\delta^{44}Ca$ that is lower than the BSE value, and all are much lower than the modern seawater value of +0.95 (Fantle and Tipper, 2014; Nielsen et al., 2011)

and the inferred seawater value of +0.5 for early Paleozoic time (Farkas et al., 2007). The mean $\delta^{44}Ca$ for Troodos is -0.23 ±0.08 and for Oman is -0.28 ±0.08. The mean Betts Cove $\delta^{44}Ca$ is lower, -0.48 ±0.19. The youngest sample measured, from ODP Site 504B, in crust that is about 6 million years old, has $\delta^{44}Ca$ = -0.22.

The epidote $^{87}Sr/^{86}Sr$ are variable between ophiolites but relatively consistent within each ophiolite locality (**Figure 1, 3**). The Late Cambrian Betts Cove epidotes have an average $^{87}Sr/^{86}Sr$ of 0.7082. The Cretaceous Troodos epidote samples are between 0.7053 and 0.7054, similar to the whole rock epidosites and the calculated Troodos hydrothermal fluid ($^{87}Sr/^{86}Sr$ =0.7053 - Bickle and Teagle, 1992). The Cretaceous Oman samples vary from 0.7043 to 0.7052, slightly lower, but overlapping, the Troodos values. All of the ophiolite epidotes have $^{87}Sr/^{86}Sr$ higher than 0.7043, which is substantially different from modern epidotes from Hole 504B that have lower $^{87}Sr/^{86}Sr \approx 0.7035$, similar to modern hydrothermal vent fluids. All of the epidotes have $^{87}Sr/^{86}Sr$ greater than the local unaltered rock (Alt and Teagle, 2000; Bickle and Teagle, 1992; Turchyn et al., 2013), indicating that in all cases the hydrothermal fluid has retained some Sr isotopic 'memory' of seawater. In the Betts Cove ophiolite the local rocks are overprinted by greenschist facies metamorphism, however the epidote $^{87}Sr/^{86}Sr$ values are greater than that of the estimated unaltered boninite crust (Turchyn et al., 2013).

Because the $^{87}Sr/^{86}Sr$ of ancient seawater is variable (e.g. McArthur et al., 2001), we also provide in Table 1 the calculated fraction seawater strontium for each epidote sample, which is given by:

$$f_{Sr,SW} = \frac{^{87}Sr/^{86}Sr_{SW} - ^{87}Sr/^{86}Sr_{epidote}}{^{87}Sr/^{86}Sr_{SW} - ^{87}Sr/^{86}Sr_{rock}} \quad (2)$$

where $f_{Sr,SW}$ is the fraction seawater strontium in epidotes, $Sr_{epidote}$, $Sr_{SW}$ and $Sr_{rock}$ are the $^{87}Sr/^{86}Sr$ ratios of measured epidotes, contemporaneous paleo-seawater and the local unaltered

253 oceanic basalt respectively. The $^{87}Sr/^{86}Sr$ of unaltered basalt for the Troodos samples is 0.7037,
254 (Bickle and Teagle, 1992), and for the Oman ophiolite 0.70295 (McCulloch et al., 1980). The
255 $^{87}Sr/^{86}Sr$ of unaltered oceanic basalt at Betts Cove is more difficult to constrain, however, a
256 gabbro from the Bay of Islands ophiolite has $^{87}Sr/^{86}Sr = 0.70254$ and provides the best local
257 estimate (Jacobsen and Wasserburg, 1979). The fraction of seawater Sr for the Troodos, Oman
258 and Betts Cove samples is in general higher than that for the 504B sample, and for average
259 modern vents fluids ($f_{Sr,SW} = 0.20$). These differences are as expected because of the difference
260 in paleoseawater Ca, Sr, and $SO_4$ concentrations, but there is little correspondence between
261 $\delta^{44}Ca$ and $f_{Sr,SW}$.

262 The $^{87}Sr/^{86}Sr$ of the epidote from Hole 504B (0.70407) is higher than that of other
263 epidotes from the drill core 0.7034-0.7038 (Teagle et al., 1998), but lower than anhydrite from
264 stratigraphically above and below the sampled interval (Teagle et al., 1998). The 504B $^{87}Sr/^{86}Sr$
265 values are within the range of hydrothermal vent fluids from the nearby East Pacific Rise,
266 which have $^{87}Sr/^{86}Sr$ of 0.70285 to 0.70465 with an average $^{87}Sr/^{86}Sr$ value of 0.7038 (Bach and
267 Humphris, 1999; Palmer and Edmond, 1989). The similarity of $^{87}Sr/^{86}Sr$ values of epidotes from
268 epidote-quartz veins in Hole 504B and from other oceanic boreholes to those of modern vent
269 fluids, as well as the association of epidote with quartz plus sulfide mineralization in Hole
270 504B, has been taken to indicate that vein epidotes (and epidosite epidote) precipitate from
271 fluids similar to modern black smokers, and record the Sr isotopic composition of the vent
272 fluids (Alt, 1995a; Harris et al., 2015; Teagle et al., 1998). Additionally, the epidosites directly
273 underlie ophiolite-hosted volcanic massive sulfide deposits (e.g. Troodos and Betts Cove) and
274 are impoverished in base metals (Cu) that are enriched in the overlying sulfides. The sulfide
275 deposits are thought to be ancient analogues of black smokers (Richardson et al., 1987).

## 5. Discussion

Our primary finding is that the $\delta^{44}Ca$ of epidosites from both young seafloor and ancient ophiolites are lower than the $\delta^{44}Ca$ of BSE and the likely $\delta^{44}Ca$ of high temperature hydrothermal fluids (discussed below). The average inferred fractionation value ($\Delta^{44}Ca_{ep\text{-}fl}$) is between about -0.2 and -0.6, which is not large, but it is outside of analytical uncertainty. In the remainder of the discussion we evaluate the constraints on hydrothermal fluid $\delta^{44}Ca$, both for modern and ancient seafloor systems. High temperature mineral-fluid Ca isotope fractionation could be an equilibrium or kinetic effect. If it is kinetic, it is of general interest because until now there has been little evidence that hydrothermal minerals formed at 300-400°C show significant kinetic isotope- or trace element effects. If it is equilibrium then that requires thermodynamic conditions where the bond strength of Ca in epidote would need to be weaker than that associated with dissolved Ca in the hydrothermal solutions. We provide evidence that the equilibrium fractionation factor for epidote-fluid ($\Delta^{44}Ca_{eq}$) should be approximately zero.

### *5.1 Calcium isotopic composition of modern oceanic crust*

As noted above, recent studies have established that mantle peridotite (or specifically lherzolite), from which the rocks of the oceanic crust are derived by extensive partial melting, has $\delta^{44}Ca = 0.0$ with a small uncertainty (**Figure 2**). These studies also show that the individual minerals, especially those with low concentrations of Ca (olivine and orthopyroxene) have positive $\delta^{44}Ca$. Orthopyroxene in particular can have $\delta^{44}Ca$ up to +1.2, although it typically contains only a few percent of the Ca in lherzolite (Chen et al, 2019; Wang et al., 2017; Kang et al., 2017). Olivine can also have positive $\delta^{44}Ca$, but it contains a vanishingly small amount of

299 Ca. The mineralogical effects are evident in the data of Chen et al (2019), who found that bulk
300 lherzolite samples have an average $\delta^{44}Ca$ very close to 0.0 on our BSE scale (**Fig. 2**), but that
301 clinopyroxene-rich samples (websterite and clinopyroxenite) have slightly lower values of
302 about -0.1.

303 Theoretically, because orthopyroxene is a residual mineral during partial melting at mid-
304 ocean ridges, the derived basaltic liquid (which then becomes the oceanic crust), could have
305 $\delta^{44}Ca$ slightly below zero. To estimate the $\delta^{44}Ca$ of a model oceanic crust, we consider a partial
306 melting model, with 10% basalt liquid in equilibrium with a residue of 55% olivine, 25%
307 orthopyroxene, and 10% clinopyroxene. The calculated liquid $\delta^{44}Ca$ is -0.01 (assuming the
308 initial value for the lherzolite source rock = 0.0), based on the measured values of the minerals
309 given by Chen et al (2019). Further evolution of the liquid by crystal fractionation in a crustal
310 magma chamber to produce the dikes and flows that comprise the part of the oceanic crust that
311 hosts epidosites, is unlikely to change this significantly because the Ca in the cumulates is still
312 dominated by clinopyroxene. Thus the fractional crystallization process could drive the $\delta^{44}Ca$ of
313 the dikes and flow to values slightly higher than zero. Simon and DePaolo (2010) also reported
314 analyses of two clinopyroxene separates from ultramafic xenoliths that had values of 0.0 and -
315 0.01 relative to BSE. Measurements of $\delta^{44}Ca$ in three MORB samples reported by DePaolo
316 (2004) average +0.05 relative to BSE, also in excellent agreement with the Chen et al (2019)
317 results. The available data therefore, suggest that unaltered rocks of the oceanic crust should
318 have almost exactly the BSE value, within 0.05‰. It should be noted that extensive melting of
319 lherzolite can result in the Ca-poor residue having slightly elevated $\delta^{44}Ca$, as observed by Kang
320 et al (2019), but the derived melt will not be fractionated significantly from the value of the
321 original lherzolite.

Our conclusion is that modern oceanic crust has a narrow range of $\delta^{44}Ca$ equal to the BSE value, with a range of at most ±0.1. We do not have direct constraints on the specific oceanic crustal rocks for the Cretaceous and Late Cambrian ophiolites. Our inference is that they have the same narrow range of $\delta^{44}Ca$, and the remainder of our analysis is based on that assumption. The Betts Cove samples we analyzed, part of the Baie Verte ophiolite, is most different from typical mid-ocean ridge crust in that it has a boninitic lower crustal composition (Bédard, 1999. We are unaware of $\delta^{44}Ca$ measurements of boninites, however, the geodynamic and geochemical characteristics of boninites can be used to infer the likely $\delta^{44}Ca$. Boninites have higher MgO and $SiO_2$, are depleted in moderately incompatible trace elements and enriched in large ion lithophile trace elements compared to MORB, and are thought to form in the forearc region of subduction zones (Crawford et al., 1989). The geochemical composition of boninites suggests that they form from fluid-fluxed melting of already depleted mantle peridotite. Using the systematics of ultramafic rocks found by Kang et al. (2017), moderately refractory peridotites (depleted in clinopyroxene) might have slightly higher $\delta^{44}Ca$ than BSE (roughly +0.1). If, as suggested by Bedard (1999), the low-Ca boninites at Betts Cove were derived from large degrees of partial melting of such cpx-poor peridotite, then the boninite magma would have essentially the same $\delta^{44}Ca$ as the mantle rocks, and hence slightly higher $\delta^{44}Ca$ than BSE.

*5.2 Ca isotopic composition of modern hydrothermal fluids*

If we accept that the average $\delta^{44}Ca$ of the upper oceanic crust (basalt plus dikes especially) is zero within ±0.05‰, the next question concerns the $\delta^{44}Ca$ of the high temperature hydrothermal fluids from which the epidotes formed. There are two studies where the $\delta^{44}Ca$ of

345 modern high temperature vent fluids were measured (Amini et al., 2008; Sheuermann et al et
346 al., 2018). Amini et al (2008) report data measured on TIMS and conclude that the $\delta^{44}Ca$ of
347 fluid at the Logachev hydrothermal field is -0.05 ± 0.07 on the BSE scale. Amini et al. (2008)
348 also measured Sr isotopes and estimated a value of $^{87}Sr/^{86}Sr = 0.7034$ for the high-T fluids. The
349 22 analyses of vent fluids with Mg/Ca < 0.2 from Sheuermann et al. (2018), measured using
350 multicollector ICPMS, give the average $\delta^{44}Ca$ of hydrothermal vent fluid as -0.06 ± 0.09 (1 s.d
351 on the BSE reference scale). The Scheuermann et al. (2018) data show a total spread of 0.32
352 delta units, which is 4 times their reported 1 sigma uncertainty of ±0.08. All of the variability in
353 their data can, therefore, be ascribed to their analytical uncertainty and does not indicate scatter
354 in the $\delta^{44}Ca$ of the fluid samples. Thus, the available vent fluid data suggest that modern high
355 temperature seafloor hydrothermal fluids have a well-defined $\delta^{44}Ca \approx -0.05 \pm 0.05$, just slightly
356 lower than, but within analytical uncertainty of, both calculated and measured seafloor basaltic
357 crust and the BSE value.
358
359 *5.3 Ca isotopic composition of Cretaceous and Cambrian hydrothermal fluids*
360 The ophiolite hydrothermal fluids could have different $\delta^{44}Ca$ than the modern fluids if (1)
361 the $\delta^{44}Ca$ of the oceanic crust was different, or (2) the evolution of the fluids within the
362 hydrothermal was different enough because of the different Ca, Sr, and sulfate chemistry of the
363 contemporaneous seawater. As noted above, we assume that the oceanic crustal values are the
364 same as modern oceanic crust. The Cretaceous and Cambrian oceans had high Ca and Sr (30 –
365 35 mM and about 300 μM) and low $SO_4$ (10 mM) (Lowenstein et al., 2001, 2014; Antonelli et
366 al., 2017) which means that fluids enter the high temperature part of the system with much more
367 seawater Ca and Sr, and hence the fluid then might have had significantly higher $\delta^{44}Ca$ and

368 $^{87}Sr/^{86}Sr$ (Turchyn et al., 2013; Antonelli et al., 2017). This effect is evident in the $^{87}Sr/^{86}Sr$ of
369 ancient epidosites (Figure 1), which are significantly higher than those of modern vent fluids,
370 and is also expressed in the pattern of Sr isotope alteration in Cretaceous ophiolites (Coogan,
371 2009). However, even though there is a pronounced difference for $^{87}Sr/^{86}Sr$, the difference for
372 Ca isotopes may be small.

373 To estimate the effect of higher seawater Ca concentrations on the $\delta^{44}Ca$ in hydrothermal
374 systems, based on the seawater chemistry differences and the measured epidosite $^{87}Sr/^{86}Sr$, we
375 used the model of DePaolo (2006), which is formulated to describe flow and reaction in
376 fractured rocks (with simplifications). The model captures the effects of rapid flow through
377 fractures and slower diffusional exchange between the fracture fluid and the surrounding rock
378 matrix, a feature that is likely to be necessary to describe Sr and Ca exchange in hydrothermal
379 systems. The results of this modeling (detailed in the Appendix) are shown in Figure 3 in the
380 form of the relative evolution of $\delta^{44}Ca$ versus $^{87}Sr/^{86}Sr$ in the high temperature part of the
381 system for a simplified model where the fluid concentrations of both Ca and Sr are constant.
382 There are two sets of curves shown (Figure 3), one of which illustrates the potential effect of Ca
383 isotopic fractionation during precipitation of secondary mineral phases with negative values of
384 $\Delta^{44}Ca_{min\text{-}fluid}$..

385 The key effect of the fracture flow is that the exchange of Ca between the rock matrix
386 and the fracture fluid is slowed down relative to the exchange of Sr. For the conditions that
387 apply to seafloor hydrothermal systems, in particular typical fracture spacing that is about 2
388 meters (e.g. Nehlig, 1994; van Everdingen, 1995), the effect of fracture-matrix exchange slows
389 down Ca exchange relative to Sr exchange by a factor of approximately:

390 $$\left( \frac{Ca_{rock} / Ca_{fluid}}{Sr_{rock} / Sr_{fluid}} \right)^{1/2} \quad (3)$$

391 This factor is about 3 to 4 for the likely fluid concentration values in the ancient systems (Ca =
392 40-50 mM, Sr = 200-250 μM). The fracture effect is significant, but based on the $^{87}Sr/^{86}Sr$ of
393 the epidotes, with the exception of the Cambrian system, the fluid has ample reaction time to
394 shift Ca isotopes all the way from the seawater value of $\delta^{44}Ca$ to the value that constitutes
395 isotopic equilibrium with the rocks, as happens for the modern system (Figure 3).

396 As illustrated crudely by the dashed curves in Figure 3, if there is calcium isotope
397 fractionation, and if the Ca concentration of the fluid is not changing with time, the steady state
398 fluid $\delta^{44}Ca$ (the effective equilibrium value) is not the rock value, but rather is given by:

399 $$\delta^{44}Ca_{fluid} = \delta^{44}Ca_{rock} - \Delta^{44}Ca_{mineral-fluid} \quad (4)$$

400 However, the fluid concentrations of both Ca and Sr are generally increasing by a large factor as
401 the fluid reacts with the rocks. This means that the flux of Ca from the rock to the fluid
402 (dissolution) is larger than the flux of Ca from the fluid to the secondary minerals
403 (precipitation). If the rock-to-fluid flux is higher than the fluid-to-secondary mineral flux by a
404 factor *n*, then the above equation (representing steady state) changes to:

405 $$\delta^{44}Ca_{fluid} = \delta^{44}Ca_{rock} - \frac{\Delta^{44}Ca_{mineral-fluid}}{n} \quad (5)$$

406 For typical seafloor hydrothermal systems the value of *n* could be about 2 to 4 to explain the
407 roughly 4x increase in Ca concentration relative to seawater (and possibly 10x relative to fluids
408 affected by anhydrite precipitation), so any tendency for the fluid to exhibit calcium isotope
409 fractionation as a consequence of secondary mineral precipitation is significantly reduced. This
410 inference is supported by the available fluid data as shown in Figure 4.

411 Recent work by Sheuermann et al (2019) indicates that the anhydrite-fluid fractionation
412 factor for Ca isotopes is $\Delta^{44}Ca \approx -0.3$ at 200°C, but approaches zero above 300°C. This
413 experimental result, and the fact that observed fluid $\delta^{44}Ca$ values are close to zero, suggest that
414 overall secondary mineral calcium isotope fractionation at high temperature is negligible.
415 However, as we have discovered, epidote-fluid calcium isotope fractionation appears that it
416 could be of order $\Delta^{44}Ca \approx -0.2$ to -0.6. If this is correct, it suggests that removal of
417 hydrothermal Ca into epidote is only a small fraction of the total Ca fixed into secondary
418 minerals, and that epidote growth from hydrothermal fluids occurs farther from equilibrium and
419 with larger Ca isotope fractionation than does the growth of other Ca-bearing secondary phases.
420 as discussed in Section 5.2., the limited available vent fluid data suggest the average effective
421 $\Delta^{44}Ca$ value of secondary minerals is close to zero, with the value of +0.05 needed to fit the data
422 exactly.
423
424 *5.4 Origin of Ca isotope fractionation in hydrothermal epidotes*
425 Calcium isotope fractionation between aqueous fluids and precipitating minerals occurs
426 in three endmember regimes: equilibrium control, kinetic surface reaction control and transport
427 control (DePaolo, 2011; Lasaga, 1998). DePaolo (2011) defined the isotopic near-equilibrium
428 regime as when the mineral growth rate ($R_p$) is much less than the far-from-equilibrium
429 dissolution rate ($R_b$), such that $R_p/R_b << 1$, and when there are no transport limitations (e.g.
430 diffusion to the mineral surface). In contrast, the kinetic surface control regime occurs when the
431 net precipitation rate of a mineral exceeds the far-from-equilibrium dissolution rate ($R_p/R_b > 1$).
432 The *observed* fractionation factor for $^{44}Ca/^{40}Ca$ between epidote and fluid can be inferred
433 from the data and the models to be in the range of $\alpha_{ep\text{-}fl} = 0.9998$ to 0.9994, or in $\delta^{44}Ca$ notation,

434 $\Delta_{ep\text{-}fl}$ = -0.2 to -0.6. This of course requires that the rock values uniformly be equal to the BSE
435 value of $\delta^{44}$Ca. The uncertainty on these factors can be estimated roughly as ±0.1 plus the added
436 uncertainty on the rock values. Any isotopic fractionation is in general a combination of an
437 equilibrium component and a kinetic component. Qualitatively, it would be expected that an
438 *equilibrium* fractionation factor for epidote-fluid would be greater than unity (i.e $\alpha_{ep\text{-}fl} \geq 1$ or
439 $\Delta_{ep\text{-}fl} \geq 0$), since Ca ions should be more strongly bound, and hence have higher zero-point
440 vibrational energy, in the solid than in the fluid phase. There are few data to confirm this
441 inference. However, there are DFT calculations reported by Antonelli et al. (2019), who noted
442 that the Ca isotope fractionation of minerals can be estimated based on Ca coordination number
443 and Ca-O bond lengths. Applying their results to epidote, using a coordination number of 8 and
444 a Ca-O bond length of 2.58Å (Franz and Liebscher, 2004) yields a prediction that at equilibrium
445 at 400°C, the $\delta^{44}$Ca of epidote should be 0.20 lower than diopside and 0.22 higher than
446 plagioclase ($An_{50}$). This result predicts that the $\delta^{44}$Ca of epidote in equilibrium with a typical
447 basalt mineral assemblage of 35% diopside plus 65% plagioclase, would be essentially exactly
448 equal to the $\delta^{44}$Ca of the bulk basalt. Hence, given that the available data indicate that
449 equilibrated fluids have $\delta^{44}$Ca that is -0.05±0.05 relative to basalt, the equilibrium fractionation
450 factor for epidote must be $\Delta^{44}Ca_{eq} \approx +0.05$. This number is approximate, but suggests that the
451 equilibrium fractionation factor for epidote-fluid is barely distinguishable from $\alpha = 1.000$ (or
452 $\Delta^{44}Ca_{eq} = 0$).

453 Based on this calculation, and the evidence from the Ca isotopic composition of
454 hydrothermal fluids that no secondary Ca-bearing silicate mineral in seafloor hydrothermal
455 systems has a fractionation factor much different from $\Delta_{min\text{-}fl} = 0$, we infer that the observed
456 epidote calcium isotope fractionation is a kinetic isotope effect (KIE). It also follows that the

457 fractionation factor $\Delta_{ep\text{-}fl}$ = -0.2 to -0.6 (±0.1) represents the magnitude of the KIE at the
458 conditions of epidosite formation.

459 A kinetic isotope effect can be generated in geologic systems by surface reaction
460 limitations to mineral growth, or by transport limitations where for example, diffusive isotope
461 separation can affect the isotopic composition of the growing crystals (Watkins et al., 2017). In
462 metamorphic rocks, there is ample evidence of transport limitations, as might be expected
463 because the rocks have very low porosity and transport is mainly along grain boundaries (Wilbur
464 and Ague, 2006; Carlson, 2009). Relatively large Ca KIE's (up to 3‰) due to transport have
465 been observed in granulite facies rocks near lithologic boundaries (Antonelli et al., 2019).
466 Transport is less likely to be a limiting factor in epidote growth in fractures in a hydrothermal
467 system (or in high-porosity zones, Cann et al., 2014), so the apparent KIE we observe for
468 hydrothermal epidote is more likely to be a surface reaction effect. As formulated by DePaolo
469 (2011), the expression of a KIE during mineral growth occurs under non-equilibrium conditions.
470 Specifically, a growing mineral needs to be substantially oversaturated in the growth solution
471 such that fluxes of ions to the growing mineral surface are larger than those of the back
472 (dissolution) reaction, and the growth rate is large relative to the back reaction. The KIE is
473 predicted to be nearly fully expressed when the growth rate is more than 10 times the rate of the
474 back reaction ($R_p/R_b \geq 10$).

475 Mineral growth under supersaturated conditions, and the associated Ca KIE's, are well
476 established in the case of biogenic calcite precipitating from aqueous solutions at Earth surface
477 temperatures (e.g. Schmalz and Chave, 1963), and inorganic calcite, aragonite, and anhydrite
478 precipitating in laboratory experiments (Tang et al., 2008; Gussone et al., 2003; Watkins et al.,
479 2017; Syverson et al., 2018). Also, Amini et al (2008) inferred that anhydrite precipitating in

480 MOR hydrothermal systems is affected by calcium isotopic fractionations of order $\Delta^{44}Ca$ = -0.2
481 to -0.3. The experimental results of Syverson et al. (2018) indicate that anhydrite precipitation is
482 associated with fractionation factors of -0.1 to -0.3 at temperatures of 200°C to 300°C. Brown et
483 al (2013) found that hydrothermal calcites from the Long Valley hydrothermal system in Eastern
484 California, which also have textural evidence for rapid precipitation, have $\Delta^{44}Ca$ = -0.37 to -0.55
485 at temperatures of 150-200°C.

486 Epidote supersaturation is also directly observed in geothermal fluids. Fluids from
487 geothermal wells in Iceland where the fluid chemistry and temperatures are similar to MOR
488 systems are supersaturated in epidote (Gudmundsson and Arnórsson, 2005). Although these
489 authors concluded that the calculated epidote supersaturation was an artifact of their ionic-
490 speciation model, supersaturation of epidote in the hydrothermal fluids is also a plausible
491 interpretation of the data. There is also evidence for supersaturation of hydrothermal quartz in
492 Troodos epidosites, which have high Ti concentrations (Cann et al., 2014). If quartz is
493 supersaturated, there is a substantial likelihood that epidote is also supersaturated, considering
494 the more complex chemical composition of epidote.

495 DePaolo (2011) suggested that the back reaction rate for growing carbonate minerals
496 could be estimated from the far-from-equilibrium dissolution rate, which is a function of
497 temperature, pH, and other factors. This assumption is a good approximation for calcite; it
498 leads to close model matches for calcite $\Delta^{44}Ca$ and Sr/Ca fractionation. It is not known whether
499 the model holds for silicate precipitation, but if it did, we would expect the surface reaction KIE
500 to be expressed when the crystal growth rate is equal to or larger than the far-from equilibrium
501 dissolution rate. There are data relevant to this issue for epidote. Browne et al (1989) estimated
502 hydrothermal epidote growth rates by examining silicate ejecta from a geothermal well in New

503 Zealand. Although the constraints are not tight, they estimate growth rates of greater than 200
504 nanometers per day (>1.7 x $10^{-8}$ mol/$m^2$/sec) on the 100 crystal face at a temperature somewhat
505 above 250°C. This rate is almost 100 times faster than the laboratory-measured epidote
506 dissolution rate at 250°C based on high temperature data of Holdaway (1966) when analyzed by
507 the method of Wood and Walther (1983) and extrapolated to lower temperature using their
508 universal activation energy of 13.27 kcal/mol (2.3 x $10^{-10}$ mol/$m^2$/sec). These data suggest that
509 it is possible, and perhaps likely, that hydrothermal epidote forms under substantially
510 oversaturated conditions and at a rate high enough that it should produce KIEs. However, it
511 should also be noted that further extrapolation of the Holdaway data to 90°C using the Wood
512 and Walther method gives dissolution rates that are substantially lower than those measured by
513 Rose (1991). Interpolating between the Holdaway (1966) results and those of Rose (1991) still
514 suggests that the epidote dissolution rates at 250°C are about 10 times slower than the growth
515 rates measured by Browne et al (1989).

516 The mechanism of kinetic isotope fractionation during epidote growth from hydrothermal
517 solution can only be surmised, but there are some data that may be relevant. Hofmann et al.
518 (2014) used molecular dynamics simulations to show that the magnitude of low temperature Ca
519 KIE's (a few per mil) could be accounted for by a Ca ion mass dependence of desolvation rates
520 in water. This work has since been extended by Lammers et al. (2019). The hydration water
521 molecules associated with the light isotopes of Ca are more weakly bound and hence light Ca
522 isotopes desolvate at a higher rate than heavier isotopes. Desolvation is a required step in the
523 transfer of Ca ions from solution to the surface of a growing calcite crystal. High temperature
524 solutions also show evidence that ion solvation is important. For example, Graham and
525 Shepard (1980) saw evidence of strong ion solvation effects in solutions at 250°C to 450°C

expressed as effects in the D/H fractionation in epidotes. Seward et al. (1999) using EXAFS and MD simulations, concluded that both hydration and ion pairing can be important in concentrated chloride solutions up to 300°C. Hence, the mechanisms of Ca KIE's may be similar at both high and low temperature, and their existence and magnitudes could provide unique information about solution structure and hydrothermal crystal growth. Given that KIE may affect Ca isotope fractionation during hydrothermal mineral growth, it is also possible that O isotopes are affected, as is the case for calcite at low temperature (Watkins et al., 2013).

## 6. Conclusions

Hydrothermal epidosites from the Troodos, Oman, and Betts Cove ophiolite complexes along with epidote from epidote-quartz veins in young oceanic crust (504B) have low $\delta^{44}Ca$ compared to the estimated values for the hydrothermal fluids from which they precipitated. The magnitude of these effects is -0.2 to -0.6‰. Surface reaction kinetic isotopic effects (KIE) best explain the calcium isotope fractionation during epidote growth from hydrothermal solutions, which suggests that the fluids were supersaturated with respect to epidote and that epidote did not grow under equilibrium conditions. Similar KIE have been observed at low temperature for calcite growth from aqueous solution, and at hydrothermal conditions for calcite and anhydrite. Kinetic isotope effects during crystal growth might be common in other fluid rich mineralizing environments such as continental hydrothermal systems, porphyry copper deposits and skarns. A key implication of this study is that surface kinetic control of silicate mineral growth from aqueous solutions may be common, even at temperatures up to 400°C, and hence that silicate mineral growth in hydrothermal systems cannot be assumed to occur under near-equilibrium conditions.

**Acknowledgements**

The authors acknowledge review comments by the associate editor and three anonymous reviewers that resulted in substantial improvements to the manuscript. Support for the Berkeley Center for Isotope Geochemistry is provided by the Director, Office of Science, Office of Basic Energy Sciences, of the U.S. Department of Energy under Contract No. DE-AC02-05CH11231. This is Natural Resources Canada contribution number 20190199.

References

Alt, J.C., 1995a. Sulfur isotopic profile through the oceanic crust: Sulfur mobility and seawater-crustal sulfur exchange during hydrothermal alteration. Geology 23, 585. doi:10.1130/0091-7613(1995)023<0585:SIPTTO>2.3.CO;2

Alt, J.C., 1995b. Subseafloor Processes in Mid-Ocean Ridge Hydrothennal Systems, Seafloor Hydrothermal Systems: Physical, Chemical, Biological, and Geological Interactions, Humphris/Seafloor Hydrothermal Systems: Physical, Chemical, Biological, and Geological Interactions. American Geophysical Union (AGU), Washington, D. C. doi:10.1029/GM091p0085

Alt, J.C., Muehlenbachs, K., Honnorez, J., 1986. An oxygen isotopic profile through the upper kilometer of the oceanic crust, DSDP Hole 504B. Earth and Planetary Science Letters 80, 217–229. doi:10.1016/0012-821X(86)90106-8

Alt, J.C., Teagle, D.A.H., 2003. Hydrothermal alteration of upper oceanic crust formed at a fast-spreading ridge: mineral, chemical, and isotopic evidence from ODP Site 801. Chemical Geology 201, 191–211. doi:10.1016/S0009-2541(03)00201-8

Alt, J.C., Teagle, D.A.H., 2000. Hydrothermal alteration and fluid fluxes in ophiolites and oceanic crust. Geological Society of America Special Papers 349, 273–282. doi:10.1130/0-8137-2349-3.273

Amini, M., Eisenhauer, A., Böhm, F., Fietzke, J., 2008. Calcium isotope (δ 44/40 Ca) fractionation along hydrothermal pathways, Logatchev field (Mid-Atlantic Ridge, 14 45′ N). Geochimica et Cosmochimica Acta. doi:10.1016/j.gca.2008.05.055

Amsellem, E., Moynier, F., Puchtel, I.S., 2019, Evolution of the Ca isotopic composition of the mantle. Geochimica et Cosmochimica Acta 258, 195-206.

Antonelli, M.A., Pester, N.J., Brown, S.T., DePaolo, D.J., 2017. Effect of paleoseawater composition on hydrothermal exchange in midocean ridges. Proceedings of the National Academy of Sciences 114, 12413–12418. doi:10.1073/pnas.1709145114

586 Antonelli, M.A., Schiller, M., Schauble, E.A., Mittal, T., DePaolo, D.J., Chacko, T., Grew, E.S.,
587 Tripoli, B., 2019, Kinetic and equilibrium Ca isotope effects in high-T rocks and minerals.
588 *Earth Planet. Sci. Lett.* v. 517, 71-82
589 Armbruster, T., BONAZZI, P., AKASAKA, M., BERMANEC, V., CHOPIN, C., GIERÉ, R.,
590 HEUSS-ASSBICHLER, S., LIEBSCHER, A., MENCHETTI, S., PAN, Y., PASERO, M.,
591 2006. Recommended nomenclature of epidote-group minerals. Eur.J.Mineral. 18, 551–567.
592 doi:10.1127/0935-1221/2006/0018-0551
593 Bach, W., Fruh-Green, G.L., 2010. Alteration of the oceanic lithosphere and implications for
594 seafloor processes. ELEMENTS. doi:10.2113/gselements.6.3.173
595 Bach, W., Humphris, S.E., 1999. Relationship between the Sr and O isotope compositions of
596 hydrothermal fluids and the spreading and magma-supply rates at oceanic spreading centers.
597 Geology 27, 1067. doi:10.1130/0091-7613(1999)027<1067:RBTSAO>2.3.CO;2
598 Berndt, M.E., Seyfried, W.E., Jr, Janecky, D.R., 1989. Plagioclase and epidote buffering of
599 cation ratios in mid-ocean ridge hydrothermal fluids: Experimental results in and near the
600 supercritical region. Geochimica et Cosmochimica Acta 53, 2283–2300. doi:10.1016/0016-
601 7037(89)90351-7
602 Bédard, J.H., 1999. Petrogenesis of boninites from the Betts Cove ophiolite, Newfoundland,
603 Canada: identification of subducted source components. Journal of Petrology 40, 1853–
604 1889.
605 Bickle, M.J., Bunbury, J., Chapman, H.J., Harris, N.B.W., Fairchild, I.J., Ahmad, T., 2003.
606 Fluxes of Sr into the headwaters of the Ganges. Geochimica et Cosmochimica Acta 67,
607 2567–2584. doi:10.1016/S0016-7037(03)00029-2
608 Bickle, M.J., Teagle, D.A.H., 1992. Strontium alteration in the Troodos ophiolite: implications
609 for fluid fluxes and geochemical transport in mid-ocean ridge hydrothermal systems. Earth
610 and Planetary Science Letters 113, 219–237. doi:10.1016/0012-821X(92)90221-G
611 Bird, D.K., Spieler, A.R., 2004. Epidote in Geothermal Systems. Reviews in Mineralogy and
612 Geochemistry 56, 235–300. doi:10.2138/gsrmg.56.1.235
613 Brown, S.T., Kennedy, B.M., DePaolo, D.J., Hurwitz, S., Evans, W.C., 2013. Ca, Sr, O and D
614 isotope approach to defining the chemical evolution of hydrothermal fluids: Example from
615 Long Valley, CA, USA. Geochimica et Cosmochimica Acta 122, 209–225.
616 Browne, P.R.L., Courtney, S.F., Wood, C.P., 1989. SF and Wood, CP (1989) Formation rates of
617 calc-silicate minerals deposited inside drillhole casing, Ngatamariki geothermal field.
618 American Mineralogist 74, 759–763.
619 Cann, J.R., McCaig, A.M., Yardley, B., 2014. Rapid generation of reaction permeability in the
620 roots of black smoker systems, Troodos ophiolite, Cyprus. Geofluids.
621 doi:10.1111/gfl.12117/pdf
622 Carlson, W.D., 2011. Porphyroblast crystallization: linking processes, kinetics, and
623 microstructures. International Geology Review. doi:10.1080/00206814.2010.496184
624 Chen, C., Wei Dai, Wang, Z., Liu, Y., Li, M., Becker, H., Foley, S.F., 2019, Calcium isotope
625 fractionation during magmatic processes in the upper mantle. Geochimica et Cosmochimica
626 Acta 249, 121-137.
627 Christensen, N.I., 1978. Ophiolites, seismic velocities and oceanic crustal structure.
628 Tectonophysics 47, 131–157. doi:10.1016/0040-1951(78)90155-5
629 Church, W.R., Coish, R.A., 1976. Oceanic versus island arc origin of ophiolites. Earth and
630 Planetary Science Letters 31, 8–14. doi:10.1016/0012-821X(76)90091-1

631 Coogan, L.A., 2009. Altered oceanic crust as an inorganic record of paleoseawater Sr
632 concentration. Geochem. Geophys. Geosyst. 10, n/a–n/a. doi:10.1029/2008GC002341
633 Corliss, J.B., Dymond, J., Gordon, L.I., Edmond, J.M., Herzen, von, R.P., Ballard, R.D., Green,
634 K., Williams, D., Bainbridge, A., Crane, K., van Andel, T.H., 1979. Submarine Thermal
635 Sprirngs on the Galapagos Rift. Science 203, 1073–1083.
636 doi:10.1126/science.203.4385.1073
637 Coumou, D., Driesner, T., Heinrich, C.A., 2008. The Structure and Dynamics of Mid-Ocean
638 Ridge Hydrothermal Systems. Science 321, 1825–1828. doi:10.1126/science.1159582
639 Crawford, A.J., Falloon, T.J., Green, D.H., 1989. Classification, petrogenesis and tectonic setting
640 of boninites, in: Crawford, A.J. (Ed.), Boninites.
641 Damm, von, K.L., 2000. Chemistry of hydrothermal vent fluids from 9°–10°N, East Pacific Rise:
642 "Time zero," the immediate posteruptive period. Journal of Geophysical Research: Solid
643 Earth (1978–2012) 105, 11203–11222. doi:10.1029/1999JB900414
644 DePaolo, D.J., 2011. Surface kinetic model for isotopic and trace element fractionation during
645 precipitation of calcite fromaqueous solutions. Geochimica et Cosmochimica Acta 75, 1039–
646 1056. doi:10.1016/j.gca.2010.11.020
647 DePaolo, D.J., 2006. Isotopic effects in fracture-dominated reactive fluid–rock systems.
648 Geochimica et Cosmochimica Acta 70, 1077–1096. doi:10.1016/j.gca.2005.11.022
649 DePaolo, D.J., 2004. Calcium Isotopic Variations Produced by Biological, Kinetic, Radiogenic
650 and Nucleosynthetic Processes. Reviews in Mineralogy and Geochemistry 55, 255–288.
651 doi:10.2138/gsrmg.55.1.255
652 Dilek, Y., Furnes, H., 2014. Ophiolites and Their Origins. ELEMENTS 10, 93–100.
653 doi:10.2113/gselements.10.2.93
654 Elderfield, H., Schultz, A., 1996. Mid-ocean ridge hydrothermal fluxes and the chemical
655 composition of the ocean. Annual Review of Earth and Planetary ….
656 Fantle, M.S., DePaolo, D.J., 2007. Ca isotopes in carbonate sediment and pore fluid from ODP
657 Site 807A: The Ca2+(aq)–calcite equilibrium fractionation factor and calcite
658 recrystallization rates in Pleistocene sediments. Geochimica et Cosmochimica Acta 71,
659 2524–2546. doi:10.1016/j.gca.2007.03.006
660 Fantle, M.S., Tipper, E.T., 2014. Calcium isotopes in the global biogeochemical Ca cycle:
661 Implications for development of a Ca isotope proxy. Earth Science Reviews 129, 148–177.
662 doi:10.1016/j.earscirev.2013.10.004
663 Franz, G. and Liebscher, A., 2004, Physical and Chemical properties of Epidote Minerals.
664 Reviews in Mineralogy and Geochemistry 56, 1-82.
665 Farkasˇ J, Bohm F, Wallmann K., Blenkinsop, J., Eisenhauer, A., van Geldern, R., Munnecke,
666 A., Voigt, A., Veizer, J., 2007, Calcium isotope record of Phanerozoic oceans: implications
667 for chemical evolution of seawater and its causative mechanisms. Geochim Cosmochim Acta
668 71, 5117–5134
669 Gass, I.G., 1968. Is the Troodos Massif of Cyprus a Fragment of Mesozoic Ocean Floor? Nature
670 220, 39–42. doi:10.1038/220039a0
671 Graham, C.M. Sheppard, S.M.F., 1980, Experimental hydrogen isotope studies, II.
672 Fractionations in the systems epidote-NaCl-H2O, epidote-CaCl2-H2O and epidote-seawater,
673 and the hydrogen isotope composition of natural epidotes. Earth Planet. Sci. Lett., 49, 237-
674 251.

675 Gregory, R.T., 2003. Ophiolites and global geochemical cycles: implications for the isotopic
676 evolution of seawater. Geological Society, London, Special Publications 218, 353–368.
677 doi:10.1144/GSL.SP.2003.218.01.18
678 Gudmundsson, B.T., Arnórsson, S., 2005. Secondary mineral–fluid equilibria in the Krafla and
679 Námafjall geothermal systems, Iceland. Applied Geochemistry.
680 doi:10.1016/j.apgeochem.2005.04.020
681 Gussone, N., Böhm, F., Eisenhauer, A., Dietzel, M., Heuser, A., Teichert, B.M.A., Reitner, J.,
682 Wörheide, G., Dullo, W.-C., 2005. Calcium isotope fractionation in calcite and aragonite.
683 Geochimica et Cosmochimica Acta 69, 4485–4494. doi:10.1016/j.gca.2005.06.003
684 Harris, M., Coggon, R.M., Smith-Duque, C.E., Cooper, M.J., Milton, J.A., Teagle, D.A.H., 2015.
685 Channelling of hydrothermal fluids during the accretion and evolution of the upper oceanic
686 crust: Sr isotope evidence from ODP Hole 1256D. Earth and Planetary Science Letters 416,
687 56–66. doi:10.1016/j.epsl.2015.01.042
688 Hart, S.R., 1969. K, Rb, Cs contents and K/Rb, K/Cs ratios of fresh and altered submarine
689 basalts. Earth and Planetary Science Letters 6, 295–303. doi:10.1016/0012-821X(69)90171-
690 X
691 Hofmann, A.W., White, W.M., 1982. Mantle plumes from ancient oceanic crust. Earth and
692 Planetary Science Letters 57, 421–436. doi:10.1016/0012-821X(82)90161-3
693 Holdaway, M.J., 1966, Hydrothermal stability of clinozoisite plus quartz. Am. J. Sci. 264, 643-
694 667.
695 Huang, R., Audétat, A., 2012. The titanium-in-quartz (TitaniQ) thermobarometer: A critical
696 examination and re-calibration. Geochimica et Cosmochimica Acta 84, 75–89.
697 Huang, S., Farkaš, J., Jacobsen, S.B., 2010. Calcium isotopic fractionation between
698 clinopyroxene and orthopyroxene from mantle peridotites. Earth and Planetary Science
699 Letters 292, 337–344. doi:10.1016/j.epsl.2010.01.042
700 Humphris, S.E., Thompson, G., 1978. Hydrothermal alteration of oceanic basalts by seawater.
701 Geochimica et Cosmochimica Acta 42, 107–125. doi:10.1016/0016-7037(78)90221-1
702 Jacobsen, S.B., Wasserburg, G.J., 1979. Nd and Sr isotopic study of the Bay of Islands ophiolite
703 complex and the evolution of the source of midocean ridge basalts. Journal of Geophysical
704 …. doi:10.1029/JB084iB13p07429/pdf
705 Kang J. T., Ionov D. A., Liu F., Zhang C. L., Golovin A. V., Qin L. P., Zhang Z. F. and Huang
706 F. (2017) Calcium isotopic fractionation in mantle peridotites by melting and metasomatism
707 and Ca isotope composition of the Bulk Silicate Earth. Earth Planet. Sci. Lett. 474, 128–137
708 Karson, J., 2016. Sheeted Dike Complexes in Contemporary Oceanic Crust: Implications for
709 Spreading Processes and the Interpretation of Ophiolites. Acta Geologica Sinica 90.
710 Kay, R.W., 1980. Volcanic arc magmas: implications of a melting-mixing model for element
711 recycling in the crust-upper mantle system. The Journal of Geology. doi:10.2307/30066081
712 Kay, R.W., Sun, S.S., Lee-Hu, C.N., 1978. Pb and Sr isotopes in volcanic rocks from the
713 Aleutian Islands and Pribilof Islands, Alaska. Geochimica et Cosmochimica Acta 42, 263–
714 273. doi:10.1016/0016-7037(78)90178-3
715 Lammers, L.N., Kulasinski, K., Zarzycki, P., DePaolo, D.J., 2019, Molecular simulations of
716 kinetic stable calcium isotope fractionation at the calcite-aqueous interface. Chemical
717 Geology 532, https://doi.org/10.1016/j.chemgeo.2019.119315
718 Lasaga, A.C., 1998. Reaction Kinetics in Geoscience, 811 p.

719 Lowenstein, T.K., Timofeeff, M.N., Brennan, S.T., Hardie, L.A., Demicco, R.V., 2001.
720 Oscillations in Phanerozoic Seawater Chemistry: Evidence from Fluid Inclusions. Science
721 294, 1086–1088. doi:10.1126/science.1064280
722 MacLeod, C.J., Rothery, D.A., 1992. Ridge axial segmentation in the Oman ophiolite: evidence
723 from along-strike variations in the sheeted dyke complex. Geological Society, London,
724 Special Publications 60, 39–63. doi:10.1144/GSL.SP.1992.060.01.03
725 Matthews, A., Goldsmith, J.R., Clayton, R.N., 1983. Oxygen isotope fractionation between
726 zoisite and water. Geochimica et Cosmochimica Acta 47, 645–654. doi:10.1016/0016-
727 7037(83)90285-5
728 Matthews, A., Schliestedt, M., 1984. Evolution of the blueschist and greenschist facies rocks of
729 Sifnos, Cyclades, Greece. Contrib Mineral Petrol 88, 150–163. doi:10.1007/BF00371419
730 Mcarthur, J.M., Howarth, R.J., Bailey, T.R., 2001. Strontium isotope stratigraphy: LOWESS
731 version 3: best fit to the marine Sr-isotope curve for 0–509 Ma and accompanying look-up
732 table for deriving …. The Journal of Geology. doi:10.1086/319243
733 McCulloch, M., Gregory, R., Wasserburg, G., Taylor, H., 1980. A neodymium, strontium, and
734 oxygen isotopic study of the Cretaceous Samail ophiolite and implications for the
735 petrogenesis and seawater-hydrothermal alteration of oceanic crust. Earth and Planetary
736 Science Letters 46, 201–211. doi:10.1016/0012-821X(80)90006-0
737 Miller, D.M., Goldstein, S.L., Langmuir, C.H., 1994. Cerium/lead and lead isotope ratios in arc
738 magmas and the enrichment of lead in the continents. Nature.
739 Moores, E.M., Vine, F.J., 1971. The Troodos Massif, Cyprus and other Ophiolites as Oceanic
740 Crust: Evaluation and Implications. Philosophical Transactions of the Royal Society of
741 London A: Mathematical, Physical and Engineering Sciences 268, 443–467.
742 doi:10.1098/rsta.1971.0006
743 Nehlig, P. (1994). Fracture and permeability analysis in magma-hydrothermal transition zones in
744 the Samail Ophiolite (Oman). *Journal of Geophysical Research*, *99*(B1), 589–
745 601. https://doi.org/10.1029/93JB02569
746 Nielsen, L.C., Druhan, J.L., Yang, W., Brown, S.T., DePaolo, D.J., 2011. Calcium Isotopes as
747 Tracers of Biogeochemical Processes, in: Baskaran, M. (Ed.), Handbook of Environmental
748 Isotope Geochemistry. Springer Berlin Heidelberg, Berlin, Heidelberg, pp. 105–124.
749 doi:10.1007/978-3-642-10637-8_7
750 Palmer, M.R., Edmond, J.M., 1989. The strontium isotope budget of the modern ocean. Earth
751 and Planetary Science Letters.
752 Pearce, J.A., 2014. Immobile Element Fingerprinting of Ophiolites. ELEMENTS 10, 101–108.
753 doi:10.2113/gselements.10.2.101
754 Pester, N.J., Reeves, E.P., Rough, M.E., Ding, K., Seewald, J.S., Seyfried, W.E., Jr, 2012.
755 Subseafloor phase equilibria in high-temperature hydrothermal fluids of the Lucky Strike
756 Seamount (Mid-Atlantic Ridge, 37Â°17â€²N). Geochimica et Cosmochimica Acta 90, 303–
757 322. doi:10.1016/j.gca.2012.05.018
758 Pritchard, R.G., 1979. Alteration of basalts from DSDP Legs 51, 52, and 53, Holes 417A and
759 418A. Initial reports of the Deep Sea Drilling Project.
760 Richardson, C.J., Cann, J.R., Richards, H.G., Cowan, J.G., 1987. Metal-depleted root zones of
761 the Troodos ore-forming hydrothermal systems, Cyprus. Earth and Planetary Science Letters
762 84, 243–253. doi:10.1016/0012-821X(87)90089-6
763 Rose, N.M., 1991, Dissolution rates of prehnite, epidote and albite. Geochimica et
764 Cosmochimica Acta 55, 3273-3286

765 Salters, V.J.M., Stracke, A., 2004. Composition of the depleted mantle. Geochem. Geophys.
766 Geosyst. 5, n/a–n/a. doi:10.1029/2003GC000597
767 Scheuermann, P.P., Syverson, D.D., Higgins, J.A., Pester, N.J., Seyfried, W.E., Jr, 2018.
768 Calcium isotope systematics at hydrothermal conditions: Mid-ocean ridge vent fluids and
769 experiments in the CaSO4-NaCl-H2O system. Geochimica et Cosmochimica Acta 226, 18–
770 35. doi:10.1016/j.gca.2018.01.028
771 Schiffman, P., Smith, B.M., Varga, R.J., Moores, E.M., 1987. Geometry, conditions and timing
772 of off-axis hydrothermal metamorphism and ore-deposition in the Solea graben. Nature 325,
773 423–425. doi:10.1038/325423a0
774 Schmalz, R.F., Chave, K.E., 1963. Calcium Carbonate - Factors Affecting Saturation in Ocean
775 Waters Off Bermuda. Science 139, 1206–&. doi:10.1126/science.139.3560.1206
776 Seward, T.M., Henderson, C.M.B., Chafnock, J.M., Driesner, T., 1999; An EXAFS study of
777 solvation and ion pairing in aqueous strontium solutions to 300°C. Geochimica et
778 Cosmochimica Acta 63, 2409-2418
779 Seyfried, W.E., Ding, K., 2013. Phase Equilibria in Subseafloor Hydrothermal Systems: a
780 Review of the Role of Redox, Temperature, Ph and Dissolved Cl on the Chemistry of Hot
781 Spring Fluids at Mid-Ocean Ridges, Seafloor Hydrothermal Systems: Physical, Chemical,
782 Biological, and Geological Interactions, Humphris/Seafloor Hydrothermal Systems:
783 Physical, Chemical, Biological, and Geological Interactions. American Geophysical Union
784 (AGU), Washington, D. C. doi:10.1029/GM091p0248
785 Seyfried, W.E., Jr, Mottl, M.J., 1982. Hydrothermal alteration of basalt by seawater under
786 seawater-dominated conditions. Geochimica et Cosmochimica Acta 46, 985–1002.
787 doi:10.1016/0016-7037(82)90054-0
788 Seyfried, W.E., Jr., Pester, N.J., Ding, K., Rough, M., 2011. Vent fluid chemistry of the Rainbow
789 hydrothermal system (36Â°N, MAR): Phase equilibria and in situ pH controls on
790 subseafloor alteration processes. Geochimica et Cosmochimica Acta 75, 1574–1593.
791 doi:10.1016/j.gca.2011.01.001
792 Staudigel, H., 2003. Hydrothermal alteration processes in the oceanic crust. Treatise on
793 geochemistry 511–535. doi:10.1016/B0-08-043751-6/03032-2
794 Staudigel, H., Hart, S.R., 1983. Alteration of basaltic glass: Mechanisms and significance for the
795 oceanic crust-seawater budget. Geochimica et Cosmochimica Acta 47, 337–350.
796 doi:10.1016/0016-7037(83)90257-0
797 Stein, C.A., Stein, S., 1994. Constraints on hydrothermal heat flux through the oceanic
798 lithosphere from global heat flow. Journal of Geophysical Research: Solid Earth (1978–
799 2012) 99, 3081–3095. doi:10.1029/93JB02222
800 Steuber, T., Veizer, J., 2002. Phanerozoic record of plate tectonic control of seawater chemistry
801 and carbonate sedimentation. Geology 30, 1123–1126. doi:10.1130/0091-
802 7613(2002)030<1123:PROPTC>2.0.CO;2
803 Syverson, D.D., Scheuermann, P., Higgins, J.A., Pester, N.J., Seyfried, W.E., Jr, 2018,
804 Experimental partitioning of Ca isotopes and Sr into anhydrite: Consequences for the cycling
805 of Ca and Sr in subseafloor mid-ocean ridge hydrothermal systems. Geochimica et
806 Cosmochimica Acta 236, 160-178.
807 Tang, J., Dietzel, M., Böhm, F., Köhler, S.J., Eisenhauer, A., 2008. Sr2+/Ca2+ and 44Ca/40Ca
808 fractionation during inorganic calcite formation: II. Ca isotopes. Geochimica et
809 Cosmochimica Acta 72, 3733–3745. doi:10.1016/j.gca.2008.05.033

Teagle, D.A.H., Alt, J.C., Halliday, A.N., 1998. Tracing the evolution of hydrothermal fluids in the upper oceanic crust: Sr-isotopic constraints from DSDP/ODP Holes 504B and 896A. Geological Society, London, Special Publications 148, 81–97. doi:10.1144/GSL.SP.1998.148.01.06

Teagle, D.A.H., Bickle, M.J., Alt, J.C., 2003. Recharge flux to ocean-ridge black smoker systems: a geochemical estimate from ODP Hole 504B. Earth and Planetary Science Letters 210, 81–89. doi:10.1016/S0012-821X(03)00126-2

Tremblay, A., Bédard, J.H., Lauzière, K., 1997. Taconian obduction and Silurian exhumation of the Betts Cove ophiolite, Canadian Appalachians. journals.uchicago.edu 105, 701–716. doi:10.1086/515976

Turchyn, A.V., Alt, J.C., Brown, S.T., DePaolo, D.J., Coggon, R.M., Chi, G., Bédard, J.H., Skulski, T., 2013. Reconstructing the oxygen isotope composition of late Cambrian and Cretaceous hydrothermal vent fluid. Geochimica et Cosmochimica Acta 123, 440–458. doi:10.1016/j.gca.2013.08.015

van Everdingen, D. a. (1995). Fracture characteristics of the Sheeted Dike Complex, Troodos ophiolite, Cyprus: Implications for permeability of oceanic crust. *Journal of Geophysical Research*, *100*(B10), 19957. https://doi.org/10.1029/95JB01575

Wang W., Zhou C., Qin T., Kang J.-T., Huang S., Wu Z. and Huang F. (2017) Effect of Ca content on equilibrium Ca isotope fractionation between orthopyroxene and clinopyroxene. Geochim. Cosmochim. Acta 219, 44–56

Watkins, J.M., Nielsen, L.C., Ryerson, F.J., DePaolo, D.J., 2013. The influence of kinetics on the oxygen isotope composition of calcium carbonate. Earth and Planetary Science Letters 375, 349–360. doi:10.1016/j.epsl.2013.05.054

Watkins, J.M., DePaolo, D.J. and Watson, E.B., 2017, Kinetic Fractionation of Non-Traditional Stable Isotopes by Diffusion and Crystal Growth Reactions. *Reviews in Mineralogy and Geochemistry*, v. 82, 85-125

White, W., 2015. Probing the Earth's Deep Interior Through Geochemistry. Geochem. Persp. 95–251. doi:10.7185/geochempersp.4.2

Wilbur, D.E., Ague, J.J., 2006. Chemical disequilibrium during garnet growth: Monte Carlo simulations of natural crystal morphologies. Geology. doi:10.1130/G22483.1

Wood, B.J., Walther, J.V., 1983. Rates of Hydrothermal Reactions. Science 222, 413–415. doi:10.1126/science.222.4622.413

Zhu, C., Lu, P., 2009. Alkali feldspar dissolution and secondary mineral precipitation in batch systems: 3. Saturation states of product minerals and reaction paths. Geochimica et Cosmochimica Acta. doi:10.1016/j.gca.2009.03.015

Figure Captions

Fig 1. Plot of $^{87}Sr/^{86}Sr$ vs $\delta^{44}Ca$ for hydrothermal epidotes. Bulk silicate earth (BSE) and modern seawater are shown for reference. Epidotes are isotopically depleted compared to both BSE and contemporary seawater.

Figure 2: Ca isotopic measurements and CaO concentrations of ultramafic rock samples as reported by Kang et al (2017) and Chen et al (2019), plotted on the Bulk Silicate Earth reference scale for $\delta^{44}Ca$. Also shown are the $\delta^{44}Ca$ values of NIST standard SRM915a and modern seawater. Rectangle at 10-12% CaO and $\delta^{44}Ca = 0.0 \pm 0.05$ is the inferred composition of basaltic oceanic crust assuming it is formed by partial melting of lherzolite with $\delta^{44}Ca = 0$. Kang et al (2017) data are all lherzolites with varying clinopyroxene content. Chen et al (2019) data are separated into lherzolite, websterite, and clinopyroxenite samples.

Fig 3. Plot of reactive transport model results for hydrothermal seawater-basalt exchange epidotes for modern seawater, Cretaceous (90Ma) seawater and Cambrian (500Ma) seawater. Solid lines are for zero fractionation of Ca isotopes into secondary minerals. Light dashed lines are for a secondary mineral fractionation factor of $\Delta^{44}Ca = -0.3$ and for n =2, representing 2x faster addition of Ca to the fluid from primary mineral dissolution than removal into secondary minerals. Also shown are the isotopic compositions inferred for the basaltic crust for modern (M), Oman (O), and Betts Cove (BC), and the range of $\delta^{44}Ca$ of high temperature hydrothermal fluids measured by Amini et al (2008) and Scheuermann et al (2018). With the minor exception of the Betts Cove location, the models suggest that the fluids will have $\delta^{44}Ca$ essentially identical to the rocks, and hence $\delta^{44}Ca \approx 0$. For Betts Cove the unusually high $^{87}Sr/^{86}Sr$ of the

epidotes suggests slower isotopic equilibration and hence a possibility the Ca isotopes retain some memory of the seawater composition. The offset between the epidote $\delta^{44}Ca$ and the model curves is interpreted as the epidote-fluid $\Delta^{44}Ca$ fractionation factor.

874

875

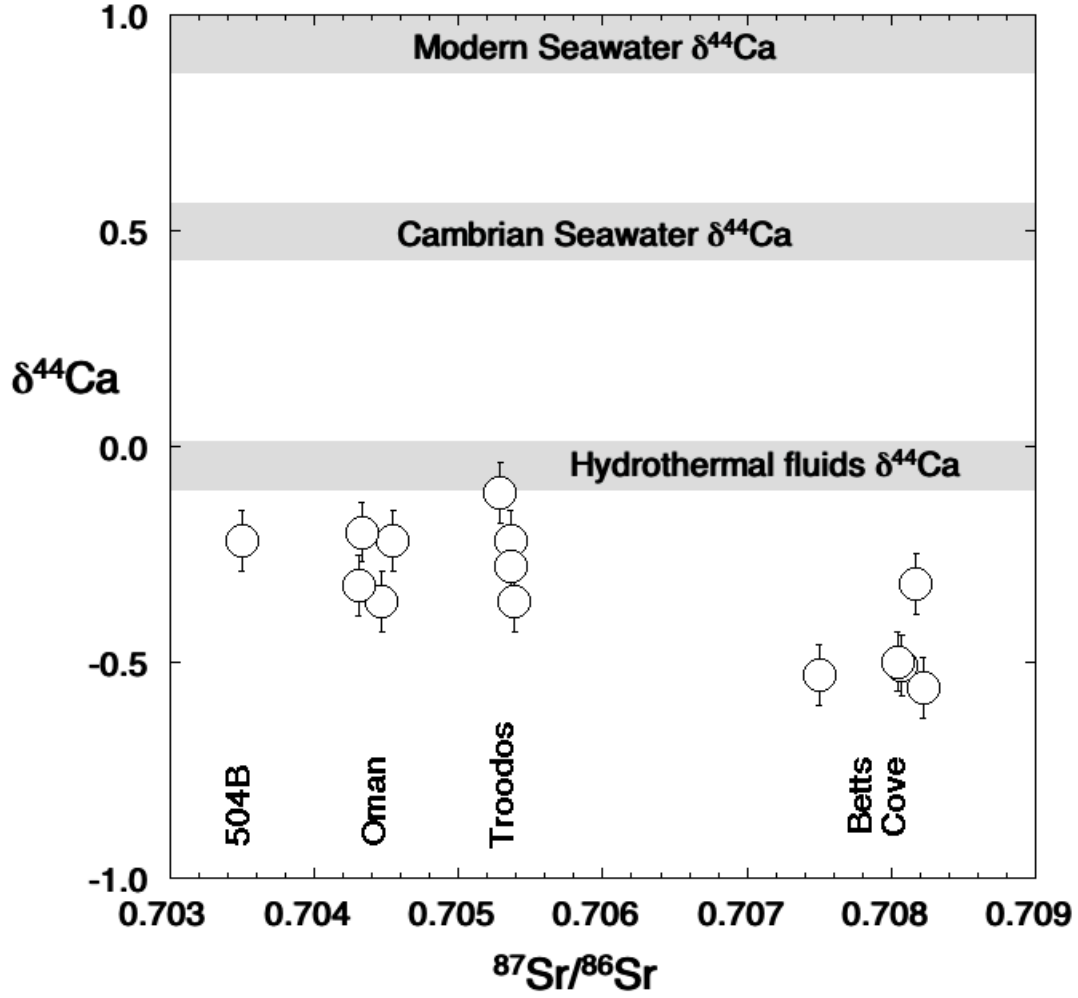


876

877 Fig 1.

878

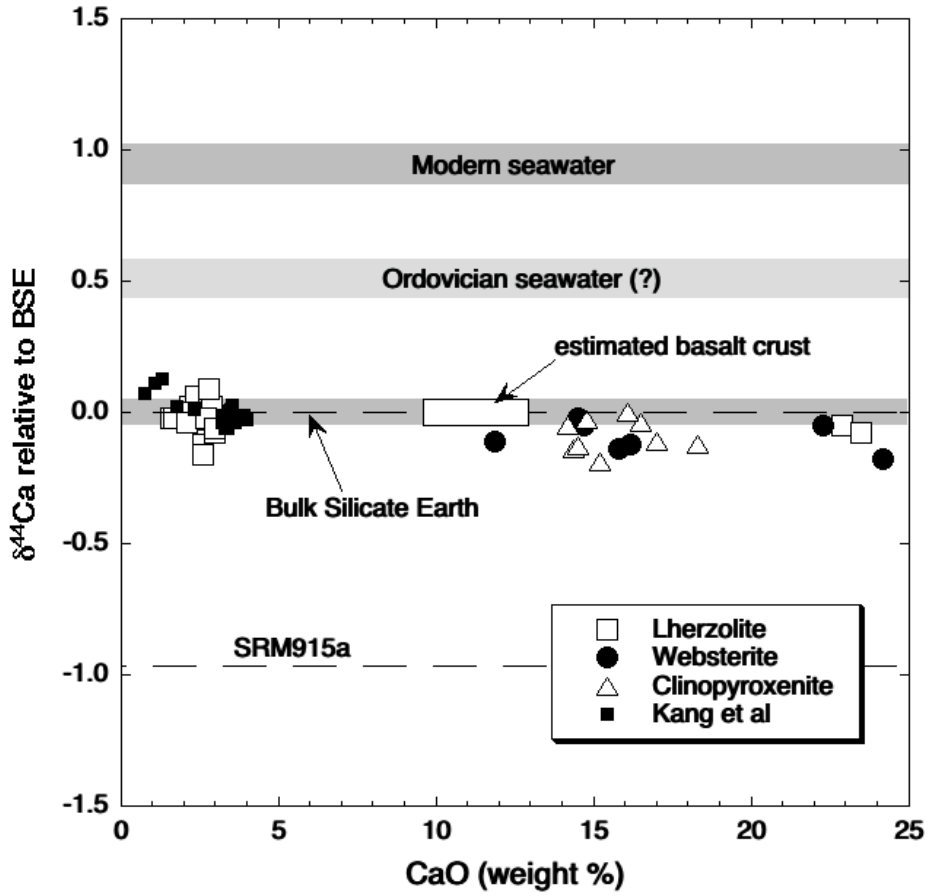


879

880 Fig 2.

881

882

883

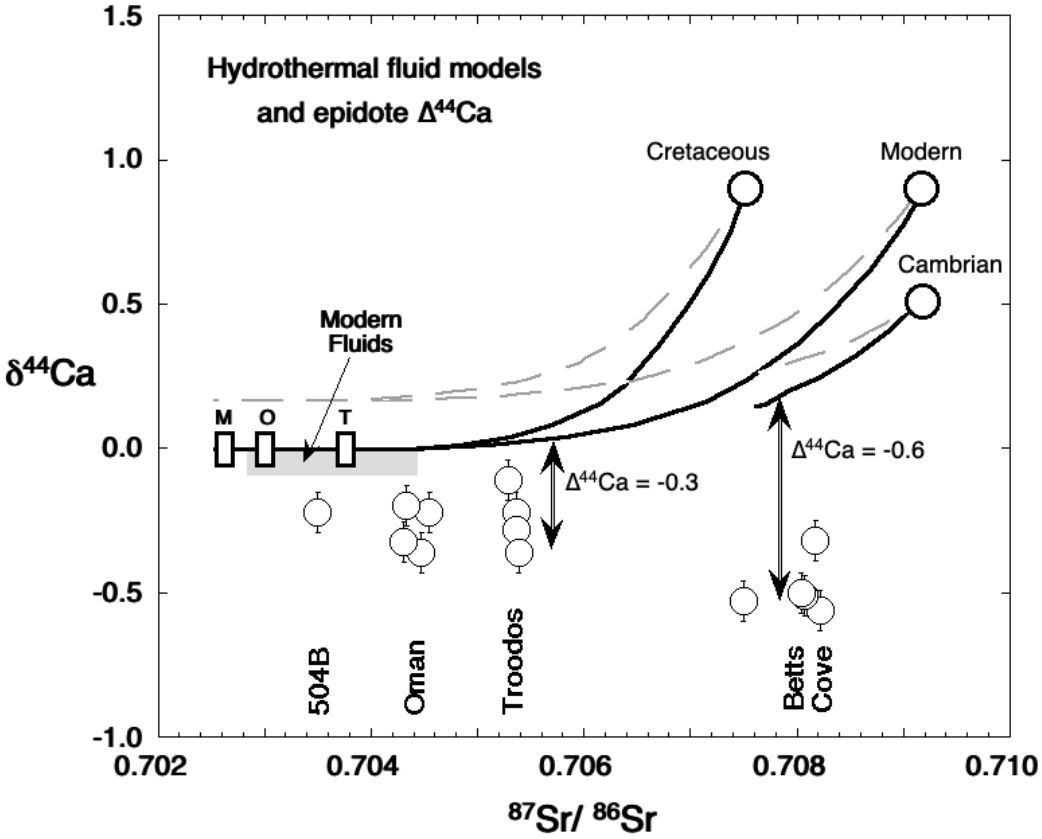


884

885 Figure 3:

886

887 Table 1.

| Sample ID | Age (Ma)[1] | Rb (ppm) | Sr (ppm) | $^{87}Rb/^{86}Sr$ | $^{87}Sr/^{86}Sr_{(m)}$[2] | 2σ | $^{87}Sr/^{86}Sr_{(t)}$[2] | $f_{Sr,SW}$ | $\delta^{18}O_{epidote}$ | $\delta^{18}O_{fluid}$ | T (°C)[3] | $\delta^{44}Ca_{BSE}$ | 2σ |
|---|---|---|---|---|---|---|---|---|---|---|---|---|---|
| TR8 | 91 | 0.055 | 469 | 0.0003 | 0.705359[(4)] | ±5 | 0.70536 | 58 | 2.9 | 1.9 | 369 | -0.22 | |
| TR18 | 91 | 0.098 | 337 | 0.0008 | 0.705293 | ±6 | 0.70529 | 57 | | | | -0.11 | 0.04 |
| TR24 | 91 | 0.070 | 700 | 0.0003 | 0.705356 | ±6 | 0.70536 | 58 | | | | -0.28 | 0.01 |
| TR26-1 | 91 | 0.059 | 531 | 0.0003 | 0.705393[(4)] | ±6 | 0.70539 | 59 | 4.2 | 2.6 | 356 | -0.36 | 0.13 |
| TR9 | 91 | 0.269 | 505 | | | | | | | | | -0.25 | 0.13 |
| TR12-1 | 91 | 0.594 | 353 | | | | | | | | | -0.23 | 0.14 |
| TR12-2 | 91 | 0.070 | 137 | | | | | | | | | -0.16 | 0.06 |
| TR17 | 91 | 0.451 | 319 | | | | | | 3.6 | 2.9 | 418 | -0.27 | 0.01 |
| TR20 | 91 | 0.510 | 542 | | | | | | | | | -0.22 | 0.03 |
| TR21 | 91 | 0.933 | 708 | | | | | | | | | -0.20 | 0.11 |
| AD28 | 95 | | 629 | | 0.704552 | ±10 | 0.70455 | 23 | | | | -0.22 | 0.10 |
| AD74 | 95 | | 2576 | | 0.705239 | ±10 | 0.70523 | 42 | | | | | |
| AD075 | 95 | | 704 | | 0.704751 | ±10 | 0.70475 | 28 | | | | | |
| AD311 | 95 | | 727 | | 0.704329 | ±10 | 0.70433 | 17 | | | | -0.20 | 0.06 |
| AD321 | 95 | | 963 | | 0.704472 | ±10 | 0.70447 | 21 | | | | -0.36 | 0.11 |
| AD330 | 95 | | 897 | | 0.704307 | ±10 | 0.70431 | 16 | | | | -0.33 | 0.10 |
| AD335 | 95 | | 849 | | 0.704461 | ±10 | 0.70446 | 21 | | | | | |
| AD339 | 95 | | 817 | | 0.704566 | ±11 | 0.70457 | 23 | | | | | |
| BC19-2 | 489 | 0.046 | 888 | 0.0002 | 0.708224 | ±6 | 0.70822 | 86 | 6.4 | 7 | 414 | -0.56 | 0.18 |
| BC 15-1 | 489 | | | | | | | | 2.3 | -0.64 | 258 | | |
| BC 20-2 | 489 | | | | | | | | 2.8 | 1.51 | 341 | | |
| BC21 | 489 | 0.093 | 382 | 0.0007 | 0.708169 | ±8 | 0.70817 | 85 | | | | -0.32 | 0.14 |
| BC33-2 | 489 | 0.908 | 646 | 0.0041 | 0.708095 | ±8 | 0.70807 | 84 | 6.5 | 5 | 344 | -0.51 | |
| BC16 | 489 | 0.032 | 212 | 0.0004 | 0.707502 | ±6 | 0.70750 | 75 | 1.5 | -2 | 241 | -0.53 | 0.06 |
| BC33-1 | 489 | 0.081 | 750 | 0.0003 | 0.708043 | ±5 | 0.70804 | 83 | 6.9 | 6 | 288 | -0.50 | 0.03 |
| 504B 84-1, 36-40 | 6 | | 542 | | 0.704068 | ±9 | 0.70407 | 24 | | | 325[(5)] | -0.22 | |

888
889 Table footnotes: (1) Magmatic ages
890 (2) $^{87}Sr/^{86}Sr_{(m)}$ are measured, mass discrimination corrected ratios; $^{87}Sr/^{86}Sr_{(t)}$ are corrected for $^{87}Rb$ decay $\lambda_{87Rb}=1.42 \times 10^{-11}$
891 (3) Fluid temperatures calculated using thermometer of (Matthews and Schliestedt, 1984).
892 (4) Values corrected from those reported by (Turchyn et al., 2013).
893 (5) Temperature is estimated using quartz $\delta^{18}O$ from nearby epidote.